J. Cent. South Univ. (2015) 22: 638−645
DOI: 10.1007/s11771-015-2565-z

Springer

Crack initiation stress and strain of jointed rock containing multi-cracks under uniaxial compressive loading: A particle flow code approach

FAN Xiang(范祥)[1, 2], KULATILAKE P H S W[2], CHEN Xin(陈新)[3], CAO Ping(曹平)[1]

1. School of Resources and Safety Engineering, Central South University, Changsha 410083, China;
2. Rock Mass Modeling and Computational Rock Mechanics Laboratories, University of Arizona, Tucson AZ 85721, USA;
3. School of Mechanics and Civil Engineering, China University of Mining and Technology (Beijing), Beijing 100083, China

Abstract: The ratio of crack initiation stress to the uniaxial compressive strength ($S_{CI,B}/S_{UC,B}$) and the ratio of axial strain at the crack initiation stress to the axial strain at the uniaxial compressive strength ($S_{A,S_{CI,B}}/S_{A,S_{UC,B}}$) were studied by performing numerical stress analysis on blocks having multi flaws at close spacing's under uniaxial loading using PFC^{3D}. The following findings are obtained: $S_{CI,B}/S_{UC,B}$ has an average value of about 0.5 with a variability of ± 0.1. This range agrees quite well with the values obtained by former research. For joint inclination angle, β=90°, $S_{A,S_{CI,B}}/S_{A,S_{UC,B}}$ is found to be around 0.48 irrespective of the value of joint continuity factor, k. No particular relation is found between $S_{A,S_{CI,B}}/S_{A,S_{UC,B}}$ and β; however, the average $S_{A,S_{CI,B}}/S_{A,S_{UC,B}}$ seems to slightly decrease with increasing k. The variability of $S_{A,S_{CI,B}}/S_{A,S_{UC,B}}$ is found to increase with k. Based on the cases studied in this work, $S_{A,S_{CI,B}}/S_{A,S_{UC,B}}$ ranges between 0.3 and 0.5. This range is quite close to the range of 0.4 to 0.6 obtained for $S_{CI,B}/S_{UC,B}$. The highest variability of ± 0.12 for $S_{A,S_{CI,B}}/S_{A,S_{UC,B}}$ is obtained for k=0.8. For the remaining k values the variability of $S_{A,S_{CI,B}}/S_{A,S_{UC,B}}$ can be expressed within ± 0.05. This finding is very similar to the finding obtained for the variability of $S_{CI,B}/S_{UC,B}$.

Key words: jointed rock; multi flaws; uniaxial loading; PFC^{3D} model; crack initiation stress ($S_{CI,B}$); axial strain at crack initiation stress $S_{A,S_{CI,B}}$

1 Introduction

Natural rock masses generally have a large number of different size discontinuities, such as fractures, joints and faults. These discontinuities influence the mechanical and hydraulic behaviors of rock masses, such as strength, deformability and permeability. Recently, more and more engineering structures have been built in or on rock masses, such as hydropower dams, underground railway tunnels, underground oil reservoirs and natural or man-made rock slopes. It is well recognized that a good understanding of the mechanical and hydraulic behaviors of rock masses is very important to the design and construction of these rock engineering structures [1−4].

As known, it is difficult and costly to perform field tests to investigate the mechanical behavior of jointed rock masses. Therefore, laboratory tests are commonly conducted to study the influence of joint geometry configurations on the mechanical behavior of jointed blocks [5−8]. Rock is a quasi-brittle material and there is no satisfactory way to produce a large number of flaws in a rock specimen with a prescribed arrangement given by a researcher. Therefore, some rock-like materials, gypsum, PMMA (poly methyl meth acrylate), a mixture of sand, cement and water, are usually used to make jointed specimens [9−11]. In most cases, thin sheets were inserted into the rock-like materials to produce discontinuities when the specimen was molded [12−14]. Sometimes a water-jet system was used to produce open flaws [10]. The preparation of the open flaws is much easier than that of the closed flaws. Therefore, more studies incorporating open flaws have been reported in Refs. [15−20]. The crack initiation, propagation and coalescence of jointed specimens with less than three open flaws under uniaxial or biaxial compression [21−23] have been investigated by many researchers. In these

Foundation item: Project(11102224) supported by the National Natural Science Foundation of China; Project(201206370124) supported by the China Scholarship Council, China
Received date: 2013−10−20; **Accepted date:** 2014−03−18
Corresponding author: CHEN Xin, Associate Professor, PhD; Tel: +86−10−62331294; E-mail: chx@cumtb.edu.cn

studies both tensile and shear cracks have been observed [21−25]. SAGONG and BOBET [26] observed four types of crack coalescences and three types of failure modes. For a large number of flaws, CHEN et al [24] observed seven types of crack initiation patterns. PRUDENCIO and JAN [18] found three types of failure modes.

In laboratory tests, it is difficult to measure the stress around the flaws during the loading process. Numerical stress analysis is another common approach that has been used to investigate the failure mechanism and the mechanical behavior of jointed rock masses using techniques such as the FEM (finite element method), RFPA (realistic failure processing analysis), PFC (particle flow code), DDA (displacement discontinuity method), BEM (boundary element method), DEM (distinct element method), and FROCK (a hybridized indirect boundary element method) [27−33]. Particle flow code (PFC), a distinct element method first induced by CUNDALL and STRACK [34], models the mechanical behavior of rock and soils. The materials are envisioned as an assembly comprised of arbitrary spherical particles (in 3D case) or circular disks (in 2D case) in the PFC program. KULATILAKE et al [35] were the pioneers in providing a realistic calibration procedure for micro-mechanical parameters of PFC^{3D} for a contact bonded particle model. They also established a jointed rock model by using closed flaws and investigated the relation between micro-parameters and macro-parameters, and the mechanical behavior of jointed rock model under uniaxial loading. Deleting of some particles in a PFC^{2D} model is another way to generate joints in a bonded particle model; this procedure creates open flaws. LEE and JEON [10] and ZHANG and WONG [36−37] studied crack initiation, propagation and coalescence using one, two or three open flaws. Many types of crack initiation and crack coalescence observed by numerical tests have been similar to the ones observed in laboratory tests. The smooth-joint is a better way to model the mechanical behavior of a joint in PFC modeling. BAHAADDINI et al [38] used the smooth-joint in a bonded particle model to investigate the effect of joint geometrical parameters on the mechanical properties of a non-persistent jointed rock mass under uniaxial compression. Many PFC users have reported the successes, failures and difficulties encountered during PFC usage. In this work, PFC^{3D} is used to study the behavior of jointed blocks having finite size (impersistent) multi flaws with very high joint density conditions under uniaxial loading.

The stress level corresponding to initiation of the first crack is also an important parameter in understanding the mechanical behavior of jointed rock. However, very little attention has been paid to studying this aspect. The ratio of crack initiation stress to failure stress may be an important parameter in rock engineering design. MARTIN and CHANDLER et al [39] obtained a range for this parameter in their study on progressive fracture of Lac du Bonnet granite. BRACE et al [40] also found a range for the same parameter in their study of dilatancy in fracture of crystalline rocks. In addition, the ratio of axial strain at the crack initiation stress level to that at failure stress level is also can be regarded as an important parameter with respect to rock engineering design. It is difficult to find data for this parameter from the published literature. Therefore, these two parameters are studied in detail in this work.

2 An introduction to PFC^{3D}, calibration of micro-mechanical parameters and setting up of jointed block model

2.1 A brief introduction to PFC^{3D}

Particle flow code (PFC) [41] developed by itasca consulting group, is a distinct element method program, which is used to model physical problems that are concerned with the movement and interaction of spherical particles. It is also possible to create particles of arbitrary shape by attaching two or more particles together, such that each group of particles acts as an autonomous object. The particle assembly is created at a given uniform size-distribution or Gaussian size-distribution with radii in the range of the minimum radius to maximum radius set by the user. The particle flow code model is composed of distinct particles that displace independent of one another, and interact only at contacts or interfaces between particles. A bonded particle model should satisfy the following assumptions. 1) The particles are treated as rigid bodies; 2) The contacts occur over a vanishingly small area; 3) Behavior at the contacts uses a soft-contact approach where the rigid particles are allowed to overlap one another at contact points; 4) The magnitude of the overlap is related to the contact force via the force-displacement law, and all overlaps are small in relation to particle sizes; 5) Bonds can exist at contacts between particles; 6) All particles are spherical. However, the clump logic supports the creation of super-particles of arbitrary shape. Each clump consists of a set of overlapping particles that acts as a rigid body with a deformable boundary.

Two types of walls including infinite walls and finite walls are provided in the PFC^{3D} program. The walls are usually used to apply boundary conditions or as loading platens. Two bonding behaviors are embodied in contact bonds and parallel bonds, both of which can be envisioned as a kind of glue joining the two neighboring particles. A contact bond also can be envisioned as a pair of elastic springs with constant normal and shear stiffness acting at the contact point. The two springs located between two neighboring particles have specified

shear and normal strength, and control the micro-mechanical behavior of a contact bond. If the magnitude of the tensile normal contact force equals or exceeds the normal contact bond strength, the bond breaks, and both the normal and shear contact forces are set to zero. If the magnitude of the shear contact force equals or exceeds the shear contact bond strength, the bond breaks, but the contact forces are not altered, it is provided that the shear force does not exceed the friction limit, and the normal force is compressive.

A contact bond model was used in the work to model the micro-mechanical behavior of a rock-like material. The contact-bond model has five micro-mechanical parameters listed in Table 1. The micro-mechanical parameters are related to the macro-mechanical behavior of the intact material. Even though some equations are given in the PFC^{3D} manual, no solid theory exists to calibrate micro-mechanical parameters by knowing the macro-mechanical properties. The calibration has to be done through a trial and error procedure. Generally, the contact elastic modulus is directly related to the elastic modulus of bonded particle model, and the shear strength and normal strength of contact-bond are directly related to the strength of bonded particle model.

A "joint generator" is provided the properties of contacts that lie along the track of a prescribed set of planes, which are assumed to be superimposed on the particle assembly. In this way, the model may be traversed by set of weak planes such as rock joints. The calculation method (DEM) is a time-stepping, explicit scheme. Modeling with PFC^{3D} involves the execution of thousands of time steps. At each step, Newton's second law (force equals mass times acceleration) is integrated twice for each particle to provide updated velocities and new positions, giving a set of contact forces acting on the particle. For further details on the PFC^{3D} the reader is referred to the user's manual [41].

Table 1 Used micro-mechanical parameters to model intact material behavior

Parameter	Meaning
E_c	Contact elastic modulus at each particle−particle contact point
k_n/k_s	Ratio of particle contact normal to shear stiffness
μ	Particle friction coefficient
σ_c	Normal strength
τ_c	Shear strength

2.2 Calibration of micro-mechanical parameters

The schematic in Fig. 1(a) is used to display the dimensions of the experimental sample. The bonded particle model performing the numerical test of intact material is shown in Fig. 1(b). The yellow grains seen in the model are spherical particles. When the micro-mechanical parameter values listed in Table 2 were employed in the numerical model, the macro-mechanical parameter values obtained from the numerical simulations were found to be in excellent agreement with that obtained from laboratory tests as listed in Table 3. Half the thickness of the experimental specimen was

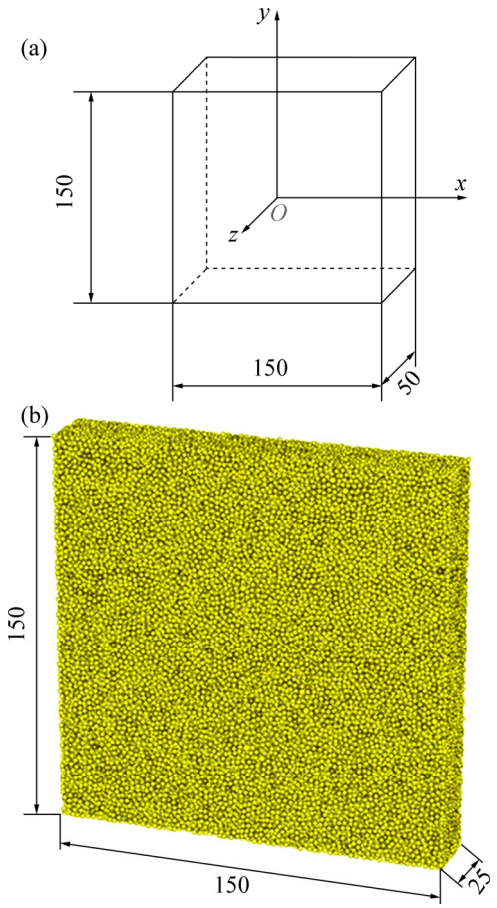

Fig. 1 Dimensions of specimen used to conduct experiments and perform numerical modeling on intact material (Unit: mm): (a) Specimen used for experiment; (b) Specimen used for numerical modeling

Table 2 Micro-mechanical parameter values used to model intact material behavior

Parameter	Value
Minimum radius/mm	0.85
Radius multiplier	1.66
Density/(kg·m^{-3})	1158.4
M	0.5
E_c/GPa	6
k_n/k_s	2.5
Normal strength, $c_{b\_sn\_mean}$/MPa	4.0
Standard deviation of normal strength, $c_{b\_sn\_sdev}$/MPa	0.8
Shear strength, $c_{b\_ss\_mean}$/MPa	6.4
Standard deviation of shear strength, $c_{b\_ss\_sdev}$/MPa	1.28

Table 3 Comparison of experimental and numerical results

Parameter	S_{UC}/MPa	E/GPa
Experimental result	8.13	4.04
Numerical result	8.26	4.03

used in the specimen used for numerical modeling. This was done to reduce the computational time. The effect of this reduction in thickness on the calculation results of uniaxial compressive strength (S_{UC}) and the elastic modulus was found to be negligible. Therefore, the micro-mechanical parameter values given in Table 2 were used in the numerical simulation tests described in the following sections.

2.3 Salient features of studied jointed blocks by numerical modeling

The joint configurations studied in this work are based on Ref. [12]. The following two parameters are used to design the joint geometry configurations in the studied blocks, joint inclination angle, β, and joint continuity factor, k. The joint configuration for β=0° is shown in Fig. 2(a). The other joint configurations result when the block is rotated around z-axis in the counter-clockwise direction at each increment of 15° until the inclination angle reaches 90° (Fig. 2(b)). When L_j, the length of a single joint, takes the values of 6, 12, 18 and 24 mm, the k value takes 0.2, 0.4, 0.6 and 0.8, respectively. When β=15°, 30°, 60° and 75°, some joints close to the boundaries get truncated (Fig. 2(d)). The distance d shown in Figs. 2(a) and (b) is 3 cm. In a bonded particle model, a joint is generated through changing micro-mechanical parameter values of the particles connecting to joint plane named as jointed particles. In PFC^{3D} a joint plane can be generated by assigning a dip angle and dip direction. Then, particles on each side of the joint plane can be assigned different micro-mechanical parameter values from the particles that represent the intact material. Usually, the micro-mechanical parameter values assigned to the particles that represent joints are smaller than those to the particles that represent intact material. The values used for the particles on each side of joint planes are given in Table 4. Those particles are shown in red color in Figs. 2(c) and (d).

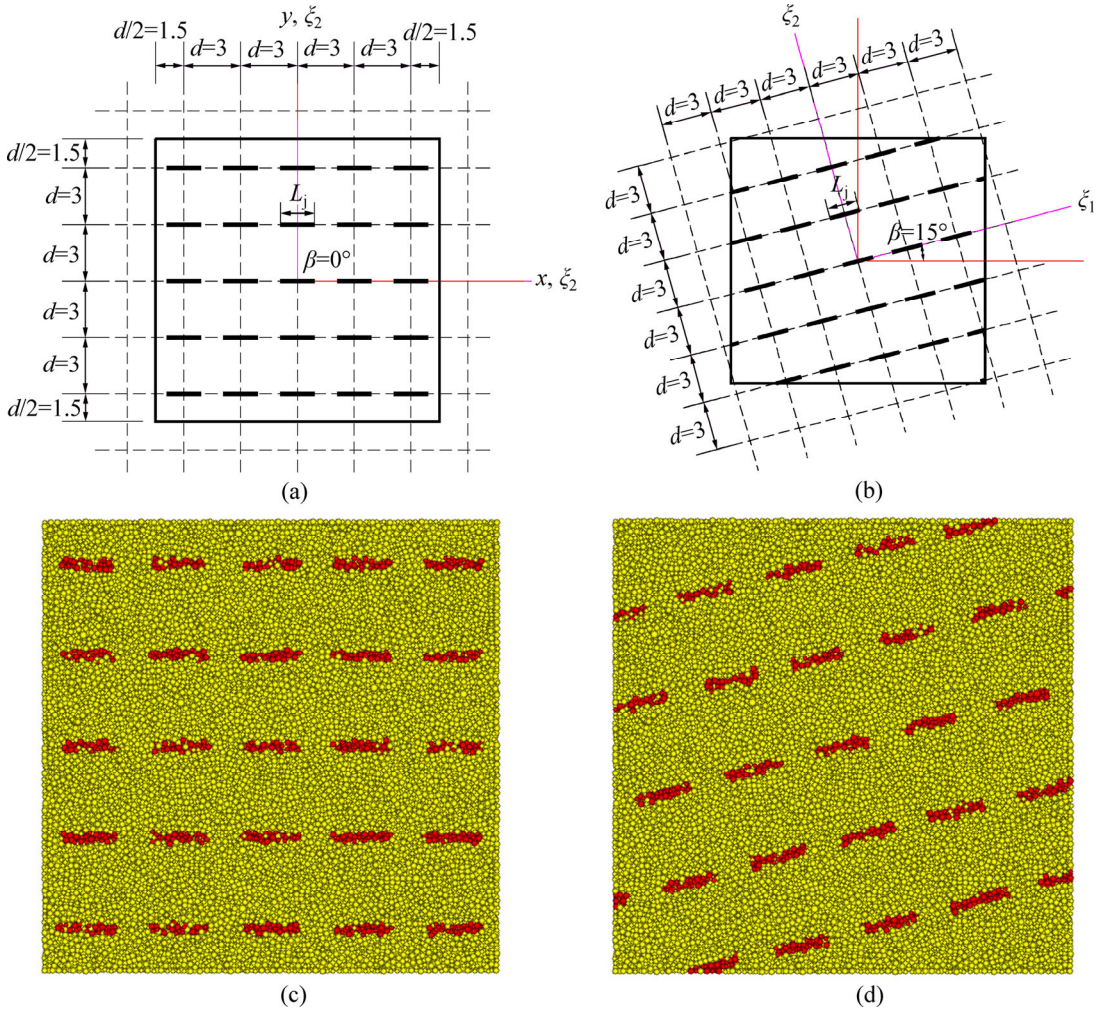

Fig. 2 Joint geometry configurations for β=0° (a, c) and β=15° (b, d)

Table 4 Micro-mechanical parameter values used for particles on each side of joint planes

Parameter	Value
Joint friction coefficient (JFC)	0.1
$k_{n,J}$/(N·m^{-1})	2.5×10^4
$k_{s,J}$/(N·m^{-1})	1.0×10^4
$s_{n,J}$/MPa	0
$s_{s,J}$/MPa	0

3 Results of uniaxial compressive strength and crack initiation stress

3.1 Effects of k and β on $S_{UC,B}$

In Fig. 3, the vertical axis is the normalized uniaxial compressive strength (UCS) of the jointed block defined as UCS of the jointed block, $S_{UC,B}$, divided by the UCS of the intact block, $S_{UC,I}$. In this work, different k values represent different joint lengths as described in Section 2.3. As shown in Fig. 3, k value significantly impacts the uniaxial compressive strength of jointed blocks for all β values apart from 90°. $S_{UC,B}/S_{UC,I}$ gradually drops with k value increasing, but the reducing magnitudes of $S_{UC,B}/S_{UC,I}$ for β=90° are very different from that for the other inclinations. The 90° specimens show a drop of about 17% on $S_{UC,B}/S_{UC,I}$ while the other inclination specimens show a drop ranging from 59% to 64% which is much higher than that of 90° samples from k=0.2 to k=0.8. The 90° specimens always have the highest uniaxial compressive strength while the 75° specimens have the second highest uniaxial compressive strength. The differences on the same k value for other five inclinations are small. In addition, Fig. 3 clearly shows that the difference between the highest strength and lowest strength on the same k value is gradually getting larger with k value changing from 0.2 to 0.8. The minimum difference for k=0.2 reaches about 7% while the maximum difference for k=0.8 reaches about 52%.

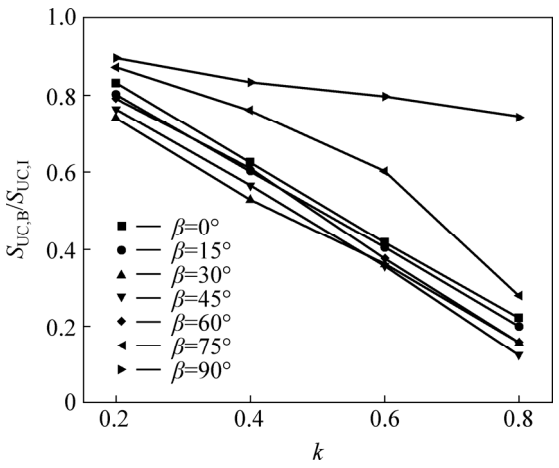

Fig. 3 $S_{UC,B}/S_{UC,I}$ vs k for different β

3.2 Effects of k and β on crack initiation stress

The crack initiation stress of jointed blocks, $S_{CI,B}$, is defined as the axial stress at which the first observation of a new crack or propagation of an existing flaw in the block is under the compressive loading. Comparison of Figs. 3 and 4 shows that with respect to the effect of β on $S_{CI,B}/S_{UC,I}$, the trend is very similar to that observed for $S_{UC,B}/S_{UC,I}$. For k=0.2, the maximum difference of $S_{CI,B}/S_{UC,I}$ among the different β values is about 0.087. This maximum difference of $S_{CI,B}/S_{UC,I}$ increases with the k value and reaches about 0.320 for k=0.8. The similar behavior of $S_{UC,B}$ and $S_{CI,B}$ with respect to k and β leads to investigating the effect of k and β on $S_{CI,B}/S_{UC,B}$. This aspect is addressed in the next section.

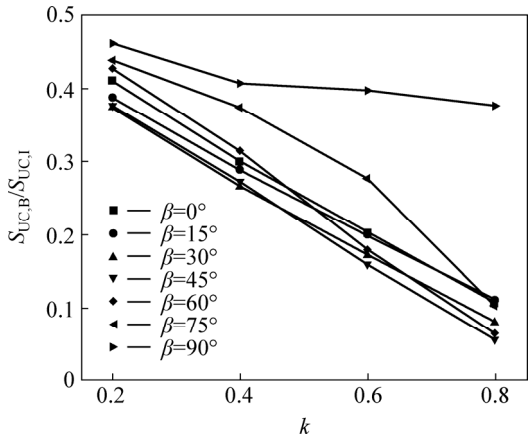

Fig. 4 $S_{CI,B}/S_{UC,I}$ vs k for different β

3.3 Effect of k and β on $S_{CI,B}/S_{UC,B}$

Some researchers have obtained values ranging in a narrow band for $S_{CI,B}/S_{UC,B}$ [39−40]. However, it is shows that the narrow bands obtained through different methods are different. One study has reported that the crack initiation occurred when $S_{CI,B}/S_{UC,B}$ exceeded about 0.2−0.4 [39]. The same study has stated that the crack damage has occurred at a uniaxial stress level of about 0.8 of the failure stress. In addition, for different loading rates, a ratio ranging from 0.35 to 0.60 was obtained for $S_{CI,B}/S_{UC,B}$ by BRACE et al [40]. This work shows that $S_{CI,B}/S_{UC,B}$ has an average value of about 0.48 with a variability of about ± 0.1 (Fig. 5). This range agrees quite well with the values obtained by BRACE et al [40]. The highest variability has been obtained for k=0.8. For the remaining k values the variability can be expressed within ± 0.05.

3.4 Effect of joint stiffness on crack initiation stress

Computations were performed for β=90° and β=45° for three different joint normal stiffness values, 2.5×10^2, 2.5×10^4 and 2.5×10^6 N/m by keeping the $k_{n,J}/k_{s,J}$ ratio equal to 2.5. For these calculations, all the other joint micro-mechanical parameter values were set to the values given in Table 4 and all the intact micro-

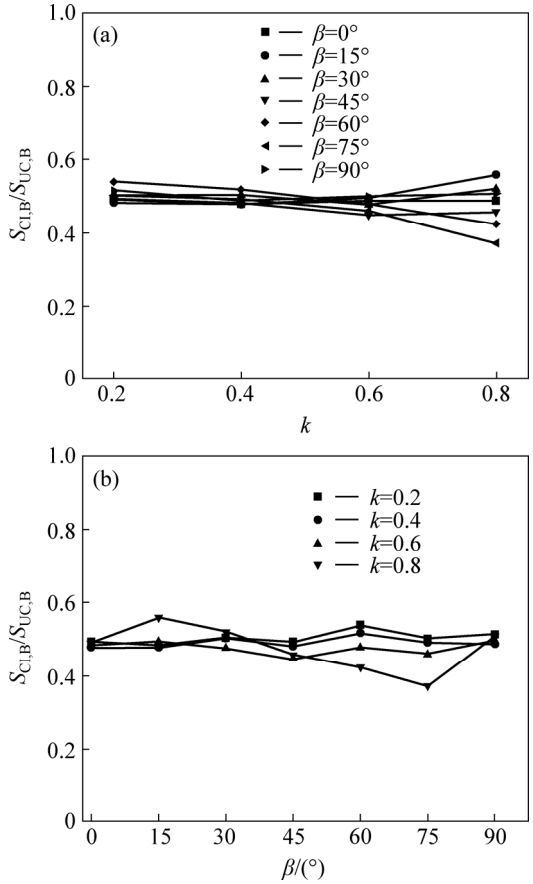

Fig. 5 Effects of k and β on $S_{CI,B}/S_{UC,B}$: (a) $S_{CI,B}/S_{UC,B}$ vs k for different β values; (b) $S_{CI,B}/S_{UC,B}$ vs β for different k values

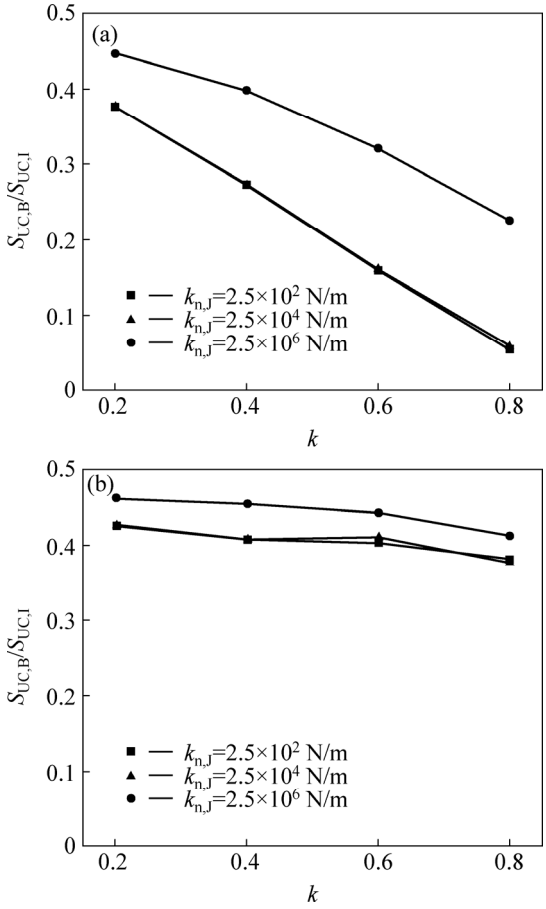

Fig. 6 Effect of joint stiffness on $S_{CI,B}/S_{UC,I}$ for different k and β values: (a) Effect of joint stiffness on $S_{CI,B}/S_{UC,I}$ for β=45°; (b) Effect of joint stiffness on $S_{CI,B}/S_{UC,I}$ for β=90°

mechanical parameter values were set as the same as given in Table 2. Figures 6(a) and (b) show that the highest $k_{n,J}$ value has resulted in a higher $S_{CI,B}/S_{UC,I}$. However, no difference has been obtained for the $S_{CI,B}/S_{UC,I}$ from the lower two $k_{n,J}$ values. Effect of β on the relation between $S_{CI,B}/S_{UC,I}$ and k was found to be the same as before given in Fig. 4. A small drop of $S_{CI,B}/S_{UC,I}$ with k was observed for β=90°; a high drop of $S_{CI,B}/S_{UC,I}$ with k was observed for β=45°.

4 Axial strain (S_A) at $S_{UC,B}$ and $S_{CI,B}$

4.1 Effects of k and β on $S_{A,S_{UC,B}}$

Figure 7 does not show any relation between S_A at $S_{UC,B}$ and β; however, it shows that the average S_A at $S_{UC,B}$ slightly decreases with increasing k. Note that the aforementioned relations are very much different from the relation between $S_{UC,B}$ and k for different β appearing in Fig. 3. Figure 7 also shows that the variability of $S_{A,S_{UC,B}}$ increases with k.

Figure 8 does not show any relation between $S_{A,S_{CI,B}}$ and β; however, it shows that the average $S_{A,S_{CI,B}}$ slightly decreases with increasing k. Note that the aforementioned relations are very much different to the relation between $S_{CI,B}$ and k for different β appearing

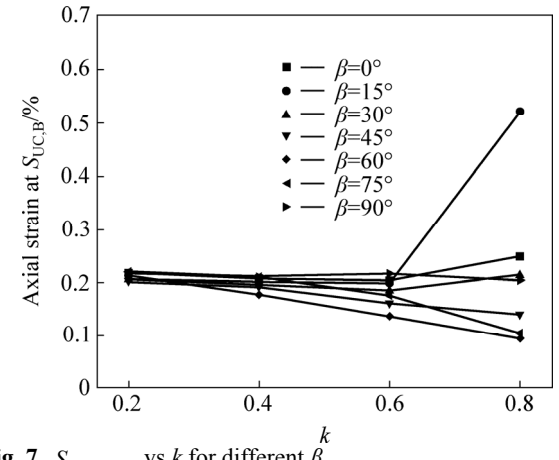

Fig. 7 $S_{A,S_{UC,B}}$ vs k for different β

in Fig. 4. Figure 8 also shows that the variability of S_A at $S_{CI,B}$ increases with k. When all the k and β cases are considered together, S_A at $S_{CI,B}$ level ranges between 0.033% and 0.126%.

4.2 Effects of k and β on $S_{A,S_{CI,B}}/S_{A,S_{UC,B}}$

Figure 9 shows that $S_{A,S_{CI,B}}/S_{A,S_{UC,B}}$ is around 0.48 irrespective of the value of k for β=90°. The same

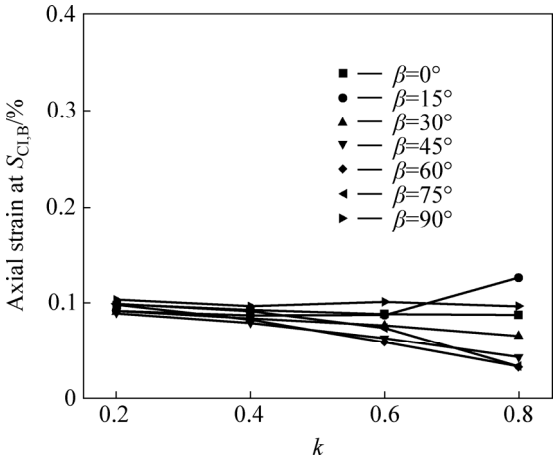

Fig. 8 $S_{A,S_{CI,B}}$ vs. k value for different β

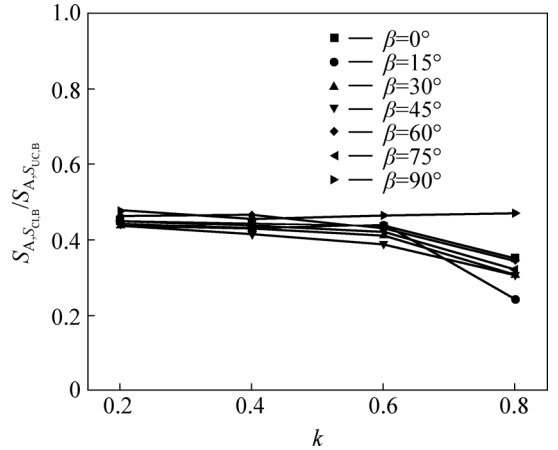

Fig. 9 $S_{A,S_{CI,B}} / S_{A,S_{UC,B}}$ vs k for different β

figure does not show any relation between $S_{A,S_{CI,B}} / S_{A,S_{UC,B}}$ and β; however, it shows that the average $S_{A,S_{CI,B}} / S_{A,S_{UC,B}}$ slightly decreases with increasing k. Figure 9 also shows that the variability of $S_{A,S_{CI,B}} / S_{A,S_{UC,B}}$ increases with k. When almost all the k and β cases are considered together, $S_{A,S_{CI,B}} / S_{A,S_{UC,B}}$ ranges between 0.3 and 0.5. Note that this range is quite close to the range of 0.4 to 0.6 obtained for $S_{CI,B}/S_{UC,B}$. The highest variability of about ±0.12 for $S_{A,S_{CI,B}} / S_{A,S_{UC,B}}$ has been resulted in for k=0.8. For the remaining k values the variability of $S_{A,S_{CI,B}} / S_{A,S_{UC,B}}$ can be expressed within ±0.05. This finding is very similar to the results obtained for the variability of $S_{CI,B}/S_{UC,B}$.

5 Conclusions

1) $S_{UC,B}/S_{UC,I}$ decreases with increasing k. β=60°, 30° and 45° provide the highest effect on the said relation. β=90° and 75° provide the lowest effect on the said relation. The moderate level effect on the mentioned relation can be seen for β=0° and 15°. $S_{UC,B}/S_{UC,I}$ shows values between 0.125 and 0.9 for the conducted study. Effect of k and β on $S_{CI,B}/S_{UC,I}$ was found to be very similar to that on $S_{UC,B}/S_{UC,I}$. The conducted study shows that $S_{CI,B}/S_{UC,B}$ has an average value of about 0.48 with a variability of ±0.1. This range agrees quite well with the values obtained by former researchers.

2) The highest joint stiffness used in the work provided a higher $S_{CI,B}/S_{UC,I}$. However, no difference was found for the $S_{CI,B}/S_{UC,I}$ from the lower two joint stiffness values. Effect of β on the relation between $S_{CI,B}/S_{UC,I}$ and k was found to be the same for different joint stiffness values. No particular relation exists between $S_{A,S_{UC,B}}$ and β; however, the average $S_{A,S_{UC,B}}$ is found to slightly decrease with increasing k. Note that the aforementioned relations are very much different to the relation between $S_{UC,B}$ and k obtained for different β. The variability of $S_{A,S_{UC,B}}$ is found to increase with k. Similar relations exist for $S_{A,S_{CI,B}}$ with k and β.

3) For β=90°, $S_{A,S_{CI,B}} / S_{A,S_{UC,B}}$ is found to be around 0.48 irrespective of the value of k. No particular relation is found between $S_{A,S_{CI,B}} / S_{A,S_{UC,B}}$ and β; however, the average $S_{A,S_{CI,B}} / S_{A,S_{UC,B}}$ seems to slightly decrease with increasing k. The variability of $S_{A,S_{CI,B}} / S_{A,S_{UC,B}}$ is found to increase with k. Based on the cases studied in this work, $S_{A,S_{CI,B}} / S_{A,S_{UC,B}}$ ranges between 0.3 and 0.5. Note that this range is quite close to the range of 0.4 to 0.6 obtained for $S_{CI,B}/S_{UC,B}$. The highest variability of ± 0.12 for $S_{A,S_{CI,B}} / S_{A,S_{UC,B}}$ is obtained for k=0.8. For the remaining k values, the variability of $S_{A,S_{CI,B}} / S_{A,S_{UC,B}}$ can be expressed within ±0.05. This finding is very similar to the finding obtained for the variability of $S_{CI,B}/S_{UC,B}$.

References

[1] DYSKIN A V, GERMANOVICH L N, USTINOV K B. A 3-D model of wing crack growth and intersection [J]. Engineering Fracture Mechanics, 1999, 63(1): 81−110.

[2] GEHLE C, KUTTER H K. Breakage and shear behavior of intermittent rock joints [J]. International Journal of Rock Mechanics & Mining Sciences, 2003, 40(5): 687−700.

[3] HOEK E, BIENIAWSKI Z T. Brittle rock fracture propagation in rock under compression [J]. International Journal of Fracture Mechanics, 1965, 1(3): 137−155.

[4] KULATILAKE P H S W, HE W, UM J, WANG H. A physical model study of jointed rock mass strength under uniaxial compressive loading [J]. International Journal of Rock Mechanics & Rock Engineering, 1997, 34(3/4): 161−165.

[5] YANG Y F, TANG C A, XIA K W. Study on crack curving and branching mechanism in quasi-brittle materials under dynamic biaxial loading [J]. International Journal of Fracture, 2012, 177(1): 53−72.

[6] SAHOURYEH E, DYSKIN A V, GERMANOVICH L N. Crack growth under biaxial compression [J]. Engineering Fracture

Mechanics, 2002, 69(18): 2187−2198.
[7] BAUD P, REUSCHLE T, CHARLEZ P. An improved wing crack model for the deformation and failure of rock in compression [J]. International Journal of Rock Mechanics Mining Sciences & Geomechanics Abstract, 1996, 33(5): 539−542.
[8] LAJTAI E Z. Brittle fracture in compression [J]. International Journal of Fracture, 1974, 10(4): 525−536.
[9] PARK C H, BOBET A. Crack coalescence in specimens with open and closed flaws: A comparison [J]. International Journal of Rock Mechanics & Mining Sciences, 2009, 46(5): 819−829.
[10] LEE H, JEON S. An experimental and numerical study of fracture coalescence in pre-cracked specimens under uniaxial compression [J]. International Journal of Solids and Structures, 2011, 48(6): 979−999.
[11] BOBET A. The initiation of secondary cracks in compression [J]. Engineering Fracture Mechanics, 2000, 66(2): 187−219.
[12] CHEN Xin, LIAO Zhi-hong, PENG Xi. Deformability characteristics of jointed rock masses under unaixal compression [J]. International Journal of Mining Science and Technology, 2012, 22(2): 213−221.
[13] KULATILAKE P H S W, PARK J, MALAMA B. A new rock mass failure criterion for biaxial loading conditions [J]. Geotecnical and Geological Engineering, 2006, 24(4): 871−888.
[14] BOBET A, EINSTEIN H H. Fracture coalescence in rock-type materials under uniaxial and biaxial compression [J]. International Journal of Rock Mechanics and Mining Sciences, 1998, 35(7): 863−888.
[15] SINGH M, RAO K S. Empirical methods to estimate the strength of jointed rock masses [J]. Engineering Geology, 2005, 77(1): 127−137.
[16] WONG R H C, CHAU K T, TANG C A, LIN P. Analysis of crack coalescence in rock-like materials containing three flaws–Part I: experimental approach [J]. International Journal of Rock Mechanics & Mining Sciences, 2001, 38(7): 909−924.
[17] WONG R H C, LIN P, TANG C A, CHAU K T. Creeping damage around an opening in rock-like material containing non-persistent joints [J]. Engineering Fracture Mechanics, 2002, 69(17): 2015−2027.
[18] PRUDENCIO M, van SINT-JAN M. Strength and failure modes of rock mass models with non-persistent joints [J]. International Journal of Rock Mechanics & Mining Sciences, 2007, 44(6): 890−902.
[19] van de STEEN B, VERVOORT A, NAPIER J A L. Numerical modelling of fracture initiation and propagation in biaxial tests on rock samples [J]. International Journal of Fracture, 2001, 108(2): 165−191.
[20] GHAZVINIAN A, SARFARAZI Y, SCHUBERT W, BLUMEL M. A study of the failure mechanism of planar non-persistent open joints using PFC2D [J]. Rock Mechanics and Rock Engineering, 2012, 45(5): 677−693.
[21] WONG R H C, EINSTEIN H H. Crack coalescence in molded gypsum and Carrara marble: Part I. macroscopic observations and interpretation [J]. Rock Mechanics and Rock Engineering, 2009, 42(3): 475−511.
[22] BOBET A, EINSTEIN H H. Numerical modeling of fracture coalescence in a model rock material [J]. International Journal of Fracture, 1998, 92(3): 221−252.
[23] TANG C A, LIN P, WONG R H C, CHAU K Y. Analysis of crack coalescence in rock-like materials containing three flaws–Part II: numerical approach [J]. International Journal of Rock Mechanics & Mining Sciences, 2001, 38(7): 925−939.
[24] CHEN Xin, LIAO Zhi-Hong, PENG Xi. Cracking process of rock mass models under uniaxial compression [J]. Journal of Central South University, 2013, 20(6): 1661−1678.
[25] de BREMAECKER J C, FERRIS M C. Numerical models of shear fracture propagation [J]. Engineering Fracture Mechanics, 2004, 71(15): 2161−2178.
[26] SAGONG M, BOBET A. Coalescence of multiple flaws in a rock-model material in uniaxial compression [J]. International Journal of Rock Mechanics & Mining Sciences, 2002, 39(2): 229−241.
[27] CHAN H C M, LI V, EINSTEIN H H. A hybridized displacement discontinuity and indirect boundary element method to model fracture propagation [J]. International Journal of Fracture, 1990, 45(4): 263−282.
[28] BOBET A. A hybridized displacement discontinuity method for mixed mode I-II-II loading [J]. International Journal of Rock Mechanics & Mining Sciences, 2001, 38(8): 1121−1134.
[29] TANG C A, KOU S Q. Crack propagation and coalescence in brittle materials under compression [J]. Engineering Fracture Mechanics, 1998, 61(3): 311−324.
[30] TANG C A, LIU H, LEE P K K, TSUIY, THAM L G. Numerical studies of the influence of microstructure on rock failure in uniaxial compression–Part I: effect of heterogeneity [J]. International Journal of Rock Mechanics and Mining Sciences, 2000, 37(4): 555−569.
[31] TANG C A, THAM L G, LEE P K K, TSUI Y, LIU H. Numerical studies of the influence of microstructure on rock failure in uniaxial compression–Part II: constraint, slenderness and size effect [J]. International Journal of Rock Mechanics and Mining Sciences, 2000, 37(4): 571−583.
[32] ZHANG Hou-quan, HE Yong-nian, HAN Li-jun, et al. Micro-fracturing characteristics in brittle material containing structural defects under biaxial loading [J]. Computational Materials Science, 2009, 46(3): 682−686.
[33] LIN P, WONG R H C, CHAU K T, TANG C A. Multi-crack coalescence in rock-like material under uniaxial and biaxial loading [C]// 4th International Conference on Fracture and Strength of Solids. Pohang, Korea, 2000, 183/187: 809−814.
[34] CUNDALL P A, STRACK O D L. A discrete numerical model for granular assembles [J]. Geotechnique, 1979, 29(1): 47−65.
[35] KULATILAKE P H S W, MALAMA B, WANG J. Physical and particle flow modeling of jointed rock block behavior under uniaxial loading [J]. International Journal of Rock Mechanics & Mining Sciences, 2001, 38(5): 641−657.
[36] ZHANG Xiao-ping, WONG L N Y. Cracking process in rock-like material containing a single flaw under uniaxial compression: A numerical study based on parallel bonded-particle model approach [J]. Rock Mechanics and Rock Engineering, 2012, 45(5): 711−737.
[37] ZHANG Xiao-ping, WONG R H C. Crack initiation, propagation and coalescence in rock-like material containing two flaws: A numerical study based on bonded-particle model approach [J]. Rock Mechanics and Rock Engineering, 2013, 46(5): 1001−1021.
[38] BAHAADDINI M, SHARROCK G, HEBBLEWHITE B K. Numerical investigation of the effect of joint geometrical parameters on the mechanical properties of a non-persistent jointed rock mass under uniaxial compression [J]. Computers and Geotechnics, 2013, 49: 206−225.
[39] MARTIN C D, CHANDLER N A. The progressive fracture of Lac du Bonnet granite [J]. International Journal of Rock Mechanics and Mining Engineering, 1994, 31(6): 643−659.
[40] BRACE W F, PAULDING B W, SCHOLZ C. Dilatancy in the fracture of crystalline rocks [J]. Journal of Geophysical Research, 1966, 71(16): 3939−3953.
[41] Itasca Consulting Group. PFC3D user's manual [R]. Minneapolis: Minnesota, USA: ICG, 2003.

(Edited by DENG Lü-xiang)